Published in final edited form as:

Neuroimage. 2016 November 1; 141: 242–249. doi:10.1016/j.neuroimage.2016.07.025.

pH-sensitive MRI demarcates graded tissue acidification during acute stroke — pH specificity enhancement with magnetization transfer and relaxation-normalized amide proton transfer (APT) MRI

Yingkun Guo[1,#], **Iris Yuwen Zhou**[1], **Suk-Tak Chan**[1], **Yu Wang**[1,2], **Emiri T. Mandeville**[3], **Takahiro Igarashi**[1], **Eng H. Lo**[3], **Xunming Ji**[2], and **Phillip Zhe Sun**[1,2,3,*]

[1]Athinoula A. Martinos Center for Biomedical Imaging, Department of Radiology, Massachusetts General Hospital and Harvard Medical School, Charlestown, MA, USA

[2]China-America Joint Neuroscience Institute, Xuanwu Hospital, Capital Medical University, Beijing, China

[3]Neuroprotection Research Laboratory, Department of Radiology and Neurology, Massachusetts General Hospital, Harvard Medical School, Charlestown, MA, USA

Abstract

pH-sensitive amide proton transfer (APT) MRI provides a surrogate metabolic biomarker that complements the widely-used perfusion and diffusion imaging. However, the endogenous APT MRI is often calculated using the asymmetry analysis (MTR_{asym}), which is susceptible to an inhomogeneous shift due to concomitant semisolid magnetization transfer (MT) and nuclear overhauser (NOE) effects. Although the intact brain tissue has little pH variation, white and gray matter appears distinct in the MTR_{asym} image. Herein we showed that the heterogeneous MTR_{asym} shift not related to pH highly correlates with MT ratio (MTR) and longitudinal relaxation rate (R_{1w}), which can be reasonably corrected using the multiple regression analysis. Because there are relatively small MT and R_{1w} changes during acute stroke, we postulate that magnetization transfer and relaxation-normalized APT (MRAPT) analysis increases MRI specificity to acidosis over the routine MTR_{asym} image, hence facilitates ischemic lesion segmentation. We found significant differences in perfusion, pH and diffusion lesion volumes (P<0.001, ANOVA). Furthermore, MRAPT MRI depicted graded ischemic acidosis, with the most severe acidosis in the diffusion lesion (−1.05±0.29%/s), moderate acidification within the pH/diffusion mismatch (i.e., metabolic penumbra, −0.67±0.27%/s) and little pH change in the perfusion/pH mismatch (i.e., benign oligemia, −0.04±0.14%/s), providing refined stratification of ischemic tissue injury.

Corresponding Author: Phillip Zhe Sun, Ph.D., Athinoula A. Martinos Center for Biomedical Imaging, Department of Radiology, MGH and Harvard Medical School, Rm 2301, CNY-149 13th Street, Charlestown, MA 02129, USA, pzhesun@mgh.harvard.edu, Tel: 617-726-4060; Fax: 617-726-7422.

#Current address: Department of Radiology, West China Second University Hospital, Sichuan University

Graphical Abstract

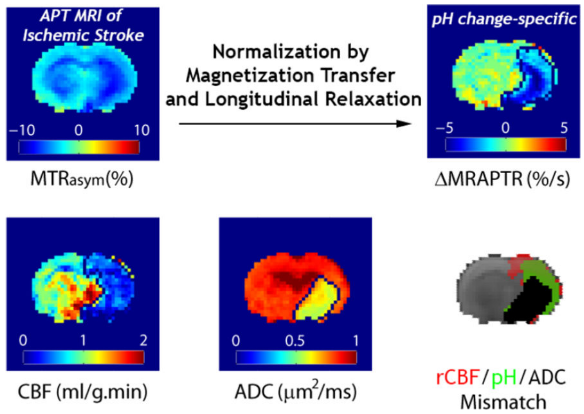

1. Introduction

Amide proton transfer (APT) MRI is promising in capturing tissue pH changes in disorders such as acute ischemia and tumor by depicting the chemical exchange saturation transfer (CEST) effect between the endogenous protein/peptide amide protons and bulk water (McVicar et al., 2014; Sheth et al., 2012; Sun and Sorensen, 2008; Sun et al., 2012; Ward et al., 2000; Zhou et al., 2003). As tissue acidosis has been postulated as a surrogate metabolic biomarker, pH imaging augments conventional MR spectroscopy (MRS)-based techniques by refining tissue classification (Chang et al., 1990; Moon and Richards, 1973; Ojugo et al., 1999). Indeed, it has been shown that pH MRI detects metabolic penumbra, complementing the commonly used perfusion and diffusion MRI for mapping metabolic disruption following ischemia (Harston et al., 2015; Sun et al., 2011b; Sun et al., 2007c).

APT MRI is often measured using the magnetization transfer (MT) asymmetry (MTR_{asym}) to compensate for RF spillover effect. In addition to pH, MTR_{asym} however, is susceptible to semisolid magnetization transfer, nuclear overhauser effect (NOE) and relaxation (Heo et al., 2016; Jokivarsi et al., 2007; Sun et al., 2005; Woessner et al., 2005). Particularly, because MT and NOE contributions are asymmetric, MTR_{asym} image is of limited pH specificity (Desmond and Stanisz, 2012; Heo et al., 2016; Sun et al., 2007b; Zhou et al., 2004; Zong et al., 2014). Although normal brain white (WM) and gray matter (GM) have similar intracellular pH (Back et al., 2000), they appear drastically different in the pH-weighted MTR_{asym} image. Consequently, it has been very challenging to resolve graded metabolic disruption within the heterogeneous perfusion/diffusion lesion mismatch (Harston et al., 2015; Sun et al., 2007c). Jin et al. estimated that the mobile amide proton concentration is about 10–20% higher in brain GM than WM (Jin et al., 2013). Concurrently, brain GM longitudinal relaxation time is slightly longer than that of WM (de Graaf et al., 2006). Hence, we postulated that concomitant saturation transfer effects (i.e., MT and NOE) and bulk water relaxation variation across the brain may contribute substantially to the pH-independent heterogeneity in the routine MTR_{asym} image, correction of which could improve the pH specificity of APT MRI. Because the relaxation and MTR changes during acute stroke are relatively small, we proposed magnetization transfer and relaxation-normalized APT (MRAPT) analysis for acute stroke imaging, in complementary to routine stroke MRI for improved stratification of graded metabolic injury.

2. Theory

The *in vivo* MTR_{asym} can be generally described by

$$MTR_{asym}=APTR+MTR'_{asym} \quad (1)$$

which includes pH-sensitive APT effect (APTR) and an intrinsic MTR asymmetry shift (MTR'_{asym}) not related to pH. The APT effect (APTR) can be described by an empirical solution (Sun and Sorensen, 2008)

$$APTR=\frac{f_{amide}*k_{amide}(pH)}{R_{1w}+f_{amide}*k_{amide}(pH)}*\alpha*(1-\sigma) \quad (2)$$

where α is the amide proton labeling coefficient, σ is the bulk water spillover factor, f_{amide} and k_{amide} are labile amide proton concentration and pH-dependent exchange rate, respectively, and R_{1w} is the bulk water longitudinal relaxation rate. For typical endogenous amide protons, because of the relatively slow amide proton exchange rate and its dilute concentration, we have $f_{amide} \cdot k_{amide} << R_{1w}$ (Sun et al., 2007b; Zhou et al., 2003). Moreover, we have $\alpha \approx 1$ and $\sigma \approx 0$ under RF irradiation level of 0.75 μT for amide proton exchange at 4.7 Tesla (Sun et al., 2012), and Eq. 1 can be simplified as

$$MTR_{asym} \approx \frac{f_{amide}*k_{amide}(pH)}{R_{1w}}+MTR'_{asym} \quad (3)$$

Hence, MRAPTR can be shown to be (Wu et al., 2012)

$$MRAPTR=R_{1w}*MTR_{asym}(pH) \ \approx f_{amide}*k_{amide}(pH)+R_{1w}*MTR'_{asym} \approx f\left(R_{1w,2w}, MTR\right) \quad (4)$$

As there is no easy means to quickly measure MTR'_{asym}, we used linear regression analysis of measurable terms such as $R_{1w,2w}$ and MTR to estimate MRAPTR, and denoted it as $f(R_{1w,2w}, MTR)$. Note that MRAPTR depends on MTR_{asym} and is pH sensitive. Because normal brain has uniform pH distribution, MRAPTR can be estimated from its linear regression relationship with MTR and R_{1w} voxel by voxel from the intact brain tissue, which accounts for the baseline MRAPTR heterogeneity and uniform brain pH. During acute stroke, the difference between the experimentally measured pH sensitive $R_{1w}*MTR_{asym}$ map and MRAPTR prediction, based on R_{1w} and MTR that show little change immediately following ischemia, should be dominated by ischemic acidosis-induced signal change. We have

$$\Delta \mathrm{MRAPTR} = \mathrm{R_{1w}} \cdot \mathrm{MTR_{asym}} - \mathrm{f}\left(\mathrm{R_{1w,2w}}, \mathrm{MTR}\right) \propto \Delta\left(\mathrm{f_{amide}} \cdot \mathrm{k_{amide}}(\mathrm{pH})\right) \quad (5)$$

We derived the change of MRAPTR with the relationship of $\Delta MRAPTR \propto f_{amide} \cdot k_{amide}$ (ΔpH), given that there is little change in amide proton concentration immediately following ischemia.

3. METHODS

3.1. Animal Stroke Model

The animal experiments have been approved by the Institutional Animal Care and Use Committee. Adult male Wistar rats (Charles River Laboratory, Wilmington, MA) were anesthetized with 1.5–2.0% isoflurane/air mixture throughout the study. Heart rate and oxygen content of blood (SpO_2) were monitored online (Nonin Pulse Oximeter 8600, Plymouth, MN), and body temperature was maintained by a circulating warm water jacket. Ten normal (n=10) and twenty acute stroke rats (n=20) following the standard intraluminal middle cerebral artery occlusion (MCAO) surgery were imaged. Briefly, after exposure of the right carotid bifurcation and suturing of the common carotid and distal external carotid arteries, a silicone-coated 4-0 nylon suture (Doccol Corp., Sharon, MA) was advanced to block the middle cerebral artery. The filament was secured and the incision was closed with sutures.

3.2. Simulation

We simulated APT effect in the presence of semi-solid MT using 3-pool Bloch-McConnell equations in Matlab (Woessner et al., 2005). To simulate how bulk water relaxation affects APTR and T_{1w}-normalzied APTR effect, we simulated typical range of T_{1w} from 1.25 to 2 s, and T_{2w} from 50 to 100 ms. Parameters we used include: exchange rates k_{amide}=30 and 10 s^{-1} for normal and ischemic pH, respectively, and k_{MT}=20 s^{-1}; concentrations f_{amide}=1/1000, f_{MT}=1/40; chemical shifts δ_{amide}=3.5 ppm, δ_{MT}=0 ppm with relaxation constants $T_{1amide,MT}$=1 s, T_{2amide}=20 ms and T_{2MT}=200 µs (Sun et al., 2007b; Zhou et al., 2003). Note that we chose a relatively long T_{2MT} similar to that used by Scheidegger et al., which allows the use of a simplified Lorentzian line shape to approximate the semi-solid MT contribution (Scheidegger et al., 2014). Because there is little overlap between NOE and APT effects, it is not necessary to include NOE in the simulation for the demonstration of relaxation-normalized APT MRI measurement (Jin et al., 2013; Zhang et al., 2016).

3.3. MRI

MRI scans were performed on a 4.7 Tesla small-bore scanner (Bruker Biospec, Erlangen Germany). Multi-slice MRI (5 slices, slice thickness/gap=1.8/0.2 mm, field of view=20×20 mm^2, image matrix=48×48) was acquired with echo-planar imaging (EPI). Our study chose a dual RF coil setup, including a 70 mm volume transmitter coil and an actively-decoupled 20 mm surface receiver coil, to simultaneously achieve homogeneous B_1 field and increased sensitivity in signal detection. In addition, we applied high order Fastmap shimming and reset the bulk water frequency using the point resolved spectroscopy (PRESS) protocol without water suppression. Diffusion MRI was obtained using single-shot isotropic diffusion-weighted MRI with two b-values of 250 and 1,000 s/mm^2 (repetition time (TR)/echo time (TE) = 3250/54 ms, 16 averages, scan time=2 min) (Mori and van Zijl, 1995). For pH-weighted APT MRI, we used the recovery time of 5,000 ms, primary RF saturation duration of 4,500 ms, and secondary RF saturation duration of 500 ms for an RF irradiation amplitude of 0.75 μT applied at ±3.5ppm (Sun et al., 2011a). The unsaturated control scan was signal-averaged 8 times, while the saturated images were averaged 32 times (scan time=4 min). T_1-weighted images were acquired using inversion recovery EPI, with seven inversion delays ranging from 250 ms to 3,000 ms (TR/TE = 6,500/15 ms, 4 averages, scan time=3 min); T_2-weigthed SE images were obtained with two TE of 30 and 100 ms (TR = 3,250 ms, 16 averages; scan time=2 min) (Cheung et al., 2012). In addition, amplitude modulated arterial spin labeling (ASL) perfusion MRI was acquired in acute stroke rats (TR/TE = 6,500/15 ms, time of saturation = 3,250 ms and 32 averages; scan time=7 min). We used B_1=4.7 μT, labeling distance of 15 mm, modulation frequency of 250 Hz (Alsop and Detre, 1998; Utting et al., 2005).

3.4. Data Analysis

Parametric T_{1w} map was obtained with mono-exponential fitting of the signal intensity as a function of the inversion time ($I(i) = I_0\lfloor 1-(1-\eta)e^{-TI_i/T_{1w}}\rfloor$), where η is the inversion efficiency and TI_i is the ith inversion time. T_{2w} and apparent diffusion coefficient (ADC) maps were calculated as $T_{2w}=\frac{\Delta TE}{\ln(I(TE_1)/I(TE_2))}$ and $ADC=\frac{\ln(I(b_1)/I(b_2))}{\Delta b}$, where $TE_{1,2}$ and $b_{1,2}$ are two TEs and diffusion b values, respectively, with ΔTE and Δb being their differences. In addition, cerebral blood flow (CBF) was derived as $CBF=\frac{\lambda(I_{ref}-I_{tag})}{2\alpha\cdot I_{ref}}\cdot\frac{e^{w/T_{1a}}}{T_{1w}}$, where I_{tag} is the label image, I_{ref} is the reference image, λ is the brain-blood partition coefficient for water, α is the degree of inversion with transient time correction, w is the post-labeling delay, and T_{1a} is the arterial blood longitudinal relaxation time. In addition, MTR was calculated as $MTR(\pm3.5ppm)=1-\frac{I(\pm3.5ppm)}{I_0}$, where I(±3.5 ppm) are the label and reference images with RF irradiation applied at ±3.5 ppm, respectively, and I_0 is the control image without RF irradiation. The mean MTR (MMTR) was calculated as the average of MTRs at ±3.5 ppm, and pH-weighted MTR_{asym} was calculated as $MTR_{asym}=\frac{I(-3.5ppm)-I(+3.5ppm)}{I_0}$. In addition, MRAPTR was calculated based on the multiple regression analysis between R_{1w}*MTR_{asym}, and R_{1w} and MMTR (i.e. MRAPTR=C_0+C_{11}*R_{1w}+C_{12}*MMTR+C_2* R_{1w}*MMTR, where Cs are regression coefficients). Note that we used MMTR instead of an individual MTR to harness the image sensitivity. In addition, ΔMRAPTR was calculated as the difference between experimentally measured R_{1w}*MTR_{asym} and MRAPTR estimated from R_{1w} and MMTR maps, using coefficients determined from the intact brain tissue (i.e. ΔMRAPTR= R_{1w}*MTR_{asym} − MRAPTR, Eq. 5). In addition, ischemic lesions in rCBF, ΔMRAPTR and ADC maps were automatically defined using a K-means clustering-based algorithm which categorized all the pixels within the brain into ischemic and normal clusters (Cheung et al., 2011).

4. Results

Fig. 1a simulates the experimental factor (i.e., α*(1-σ), B_1=0.75 μT at 4.7 Tesla, δ_{amide}=3.5 ppm) from the empirical solution (Eq. 2), as functions of T_{1w} and T_{2w}, for amide exchange rates of 30 and 10 s^{-1}, typical exchange rates under normal and acidic pH, respectively (Zhou et al., 2003). The experimental factor shows little change with relaxation and exchange rate, hence, can be treated as a constant that is near unity across the brain. Although APTR increases with exchange rate and hence pH, both APTR (Fig. 1b) and APTR contrast (i.e., ΔAPTR=APTR(k_{amide}=30 s^{-1})−APTR(k_{amide}=10 s^{-1})) between two amide exchange rates (Fig. 1c) show sizable T_{1w} dependence. In comparison, T_{1w}-normalized APTR contrast (i.e., R_{1w}* ΔAPTR) shows reduced T_{1w} dependency, with the coefficient of variation (COV) as a function of T_{1w} decreased from 9.3% (Fig. 1c) to 5.5% (Fig. 1d).

Fig. 2 shows multi-parametric images from a representative normal rat brain. T_{1w} map (Fig. 2a) appears hypointense in striatum and corpus callosum when compared to cortex. In addition, ventricle shows the highest intensity in T_{1w} due to increased water content. In comparison, T_{2w} map (Fig. 2b) appears relatively homogeneous except the hyperintensity in the piriform cortex and ventricle. MTR images at the reference frequency (MTR(−) at −3.5 ppm) and amide proton labile frequency (MTR(+) at +3.5 ppm) are shown in Figs. 2c and 2d, respectively. Corpus callosum and striatum show hyperintense in MTR maps, indicating an increased contribution of semisolid macromolecules and myelin MT. Moreover, MTR(−) shows higher intensity than MTR(+), mainly due to NOE contribution around the reference offset of −3.5 ppm and to a lesser degree, asymmetric MT effect (Heo et al., 2016). Figs. 2e and 2f show the mean MTR ([MTR(+)+MTR(−)]/2) and MTR_{asym} ([MTR(−)−MTR(+)]) maps, respectively. Note that striatum and corpus callosum appear hyperintensive in MMTR images while they display hypointensity in MTR_{asym} map. It is important to point out that there is little pH difference between normal brain WM and GM, and therefore the heterogeneity in the routine MTR_{asym} image is pH-independent, correction of which should improve specificity of APT MRI to pH (Back et al., 2000; Jin et al., 2013).

Fig. 3 evaluates pixel-wise correlation between MTR_{asym} and relaxation as well as MTR. There was significant correlation between R_{1w}-scaled MTR_{asym} and R_{1w} (Fig. 3a), R_{2w} (Fig. 3b) and MMTR (Fig. 3c). Specifically, we found R_{1w}*MTR_{asym}= 6.1% −13.0%*R_{1w} (R^2=0.79, P<0.01), R_{1w}*MTR_{asym}=5.3% − 0.4%*R_{2w} (R^2=0.42, P<0.01) and R_{1w}*MTR_{asym}= 9.6% −41.6%*MMTR (R^2=0.75, P<0.01), with the linear regression fitting shown in dashed lines. With the group analysis of all normal animals, R^2 was found to be 0.76 ± 0.04, 0.39 ± 0.08 and 0.68 ± 0.10 between R_{1w}*MTR_{asym} and R_{1w}, R_{2w} and MMTR, respectively. We further tested whether multiple regression can enhance the prediction of MTR_{asym} (STATA, StataCorp LP, College Station, TX). We found that R_{2w} is not a significant predicator, and we had R_{1w}*MTR_{asym}=−13.2% +25.6%*R_{1w} +55.7% *MMTR −115.9%*MMTR*R_{1w} (R^2=0.88, P<0.001). When all normal animals were analyzed, R^2 was 0.83±0.05, showing that the majority of the intrinsic heterogeneity in the routine

MTR_{asym} map is due to longitudinal relaxation and magnetization transfer/NOE contributions. We further tested whether the proposed MRAPT MRI reduces the intrinsic pH-independent heterogeneity. R_{1w}-scaled pH-weighted MTR_{asym} map (Fig. 3e) shows noticeable contrast between brain WM and GM. Fig. 3f shows the predicted MTR_{asym} map based on multiple regression from MT and T_{1w} images. Fig. 3g shows ΔMRAPTR image, which appears relatively homogeneous across the brain. Indeed, the contrast-to-noise ratio between the striatum and cortex decreased from 2.8±0.8 to 0.3±0.4 (Figs. 3e vs. 3g, $P<0.01$, ANOVA), which confirms the effectiveness of MRAPT analysis in the removal of intrinsic heterogeneity not related to pH in the intact brain.

We tested the MRAPT analysis during acute stroke. Parametric T_{1w} (Fig. 4a) and MMTR (Fig. 4b) maps show relatively little change immediately following ischemia. Both MTR_{asym} and relaxation-normalized MTR_{asym} maps (Figs. 4c and 4d) show hypointensity in the ipsilateral ischemic brain, indicating acidosis. However, Figs. 4c and 4d display noticeable brain WM/GM contrast over the contralateral intact brain tissue, suggesting poor pH specificity of the routine MTR_{asym} image. The MRAPTR from the contralateral normal brain can be well described with multiple regression analysis of R_{1w} and MMTR (Fig. 4e). The MRAPT analysis shows substantially improved tissue homogeneity in the contralateral normal brain, which enhances the specificity of ΔMRAPTR to pH (Fig. 4f). Indeed, acidic lesion can be reliably segmented using k-means clustering (Fig. 4f) from ΔMRAPTR image while the tissue classification in a routine MTR_{asym} map is poor (data not shown). Interestingly, the ΔMRAPTR image clearly demonstrated graded tissue acidification; the striatum was demonstrated with the most severe acidification which is concurrent with diffusion lesion, while the cortical region showed a moderate pH reduction. In comparison, CBF map (Fig. 4g) shows reduced blood flow in the ipsilateral ischemic area while diffusion MRI (Fig. 4h) depicts infarction predominantly in striatum. Fig. 4i overlays three lesion areas: diffusion lesion (black), pH/diffusion lesion mismatch (green) and perfusion/pH lesion mismatch (red).

Fig. 5 shows multi-slice perfusion, pH and diffusion lesions mismatch (Fig. 5a), and the corresponding 3D volume rendering overlaid on a structural scan from a representative acute stroke rat (Fig. 5b). Note that for the 3D view, we made the lesion colors moderately transparent so we can see through different layers of lesions, resulting in slightly fainted apparent color. We found significant differences in the volume between perfusion (323±41 mm^3), pH (229±34 mm^3) and diffusion lesions (132±52 mm^3) ($P<0.001$, repeated measures One-way ANOVA, Bonferroni post-hoc test). The conventional perfusion/diffusion mismatch paradigm (Fig. 6a) demarcates the ischemic tissue into the most severely injured diffusion lesion (Area I) and the viable perfusion/diffusion lesion mismatch (Area II). We found that the diffusion lesion has slight yet significant rCBF decrease from that of perfusion/diffusion mismatch (Paired-t test, Table 1). Notably, the diffusion lesion shows significantly worsened acidosis when compared to the perfusion/diffusion mismatch. Our work shows that the conventional perfusion/diffusion lesion mismatch is pH heterogeneous, which can be further segmented into hypoperfused acidic tissue (i.e. pH/diffusion mismatch, Area IIa) and hypoperfused tissue with little acidification (i.e. perfusion/pH mismatch, Area IIb), as illustrated in Fig. 6b. We compared rCBF, ADC and ΔMRAPTR in the diffusion lesion, pH/diffusion and perfusion/pH mismatch (Table 2a). One-way ANOVA shows significant rCBF difference only between the diffusion lesion and perfusion/pH mismatch (Areas I vs. IIb, Table 2b). Although perfusion/pH and pH/ADC mismatches show significantly higher ADC value than the diffusion lesion (Areas I vs. IIa, and I vs. IIb), the ADC value for the perfusion/pH and pH/ADC mismatches are not significantly different (Areas IIa vs. IIb). Importantly, pH MRI captures graded acidification within the ischemic lesion, progressively worsened from the perfusion/pH mismatch (i.e., benign oligemia, −0.04±0.14%/s), pH/diffusion mismatch (i.e., metabolic penumbra, −0.67±0.27%/s) to diffusion lesion (−1.05±0.29%/s, P<0.0001).

5. Discussion

Our study demonstrated that the MRAPT analysis substantially enhances imaging specificity to ischemic acidification during acute stroke, permitting refined tissue classification. We found that diffusion lesion suffers more aggravated acidification than the perfusion/diffusion lesion mismatch. Importantly, the development of MRAPT analysis allows semi-automatic lesion segmentation, which refines the heterogeneous perfusion/diffusion mismatch into hypoperfused acidic lesion (Area IIa) and hypoperfused tissue with little acidification (Area IIb) to capture graded ischemic tissue metabolic disruption. The finding of heterogeneous tissue metabolic injury is consistent with the hypothesis that the perfusion/diffusion mismatch includes not only ischemic penumbra but also benign oligemia that is not at risk to infarction (Kidwell et al., 2004; Sun et al., 2007c). It is helpful to briefly discuss and compare perfusion and pH measurements during acute stroke. Because CBF is under the influences of multiple factors including anesthesia and blood pressure regulation, we calculated the rCBF to reasonably account for such variabilities. As rCBF directly maps the severity of hypoperfusion, it is very sensitive to ischemia. Yet owing to the heterogeneous collateral flow and tissue susceptibility to ischemia, the rCBF measurement is associated with but not very specific to tissue metabolic disruption. In comparison, despite the fluctuation of cerebral perfusion and oxygen saturation, tissue pH is well regulated under the normal physiological conditions. Tissue pH shift is associated with glucose/oxygen delivery and consumption imbalance during the acute stroke (An et al., 2015; Shen et al., 2016; Shu et al., 2016; Zhu et al., 2013). Because tissue acidification is exacerbated by the reduced buffering capacity of bicarbonate and hypoperfusion, often leading to cell death and tissue damage (Siesjo, 1992), pH imaging can serve as an important surrogate metabolic imaging biomarker during acute ischemic stroke. Notably, Back et al. measured tissue pH with umbelliferone fluorescence and found that penumbral pH changes reflect the local disturbance of pH regulation and, possibly, the differential fate of penumbral tissue (Back et al., 2000). Specifically, they found that pH in the peri-infarct rim was 6.53±0.24, about 50% less when compared to the pH change in the infarct core, which decreased to 6.03±0.36. Because the amide proton exchange rate is dominantly base-catalyzed, the initial pH change will yield slightly larger APT MRI contrast change, suggesting that our results are in good agreement with previous findings (Back et al., 2000).

We would like to briefly discuss the confounding NOE contribution to pH-sensitive APT MRI in acute stroke. Jones et al. showed that in concentrated bovine serum albumin solution, both NOE and APT effects show pH dependence (Jones et al., 2013). On the other hand, Jin et al. (Jin et al., 2013) and Zhang et al. (Zhang et al., 2016) found very small NOE effect change following acute stroke. We would like to point out that Jones et al. (Jones et al., 2013) used pulsed RF saturation scheme in volunteers and tumor patients, while Jin et al. (Jin et al., 2013), Zhang et al. (Zhang et al., 2016) and our study here used continuous wave saturation in acute ischemic animals. The differences in saturation schemes, diseases of interest, and the magnitude of pH change may partially explain the different conclusions of NOE contribution, which should be explored in the future. Although the routine MTR_{asym} image includes contributions from both ±3.5 ppm, it is most likely that the APT contrast change during acute ischemia is dominated by base-catalyzed amide proton exchange at 3.5 ppm.

We used a relatively weak RF irradiation power, which balances APT and concomitant RF saturation effects at 4.7 Tesla yet not overly strong to saturate amine proton exchange that is two orders of magnitude faster than that of amide protons (Cai et al., 2012; Sun et al., 2007b). Under such conditions, simulation with and without MT pool shows that MT effect dilutes the CEST effect by about 20%. This explains why adding MT into the multiple regression (T_{1w} and MMTR) significantly improves the correlation from that using T_{1w} alone. Because the MRAPT analysis requires just an additional T_{1w} map in addition to the raw CEST data, the proposed analysis can be quickly tested for different experimental settings. Briefly, it is feasible to simultaneously adjust multiple variables, such as B_1, saturation time and repetition time to optimize the APT MRI sensitivity (Sun et al., 2013). For example, Zhao et al. demonstrated that under a short saturation duration of 500 ms, an RF power of 2 μT provides higher ΔMTR_{asym}(3.5ppm) than 1 μT (Zhao et al., 2011). It helps to keep in mind that when relatively large RF power levels are used, there may be overlapping CEST effects from multiple exchangeable groups, which requires Z spectrum acquisition and line fitting to resolve their independent contribution to enhance pH MRI. This, however, extends the scan and processing time, not desirable in the acute stroke setting.

Our study found relatively small MMTR and T_{1w} changes of under 1% and 7%, respectively, during acute ischemia, consistent with those in the previous studies (Jokivarsi et al., 2010; Makela et al., 2002). As such, MRAPT approach performs well for acute stroke imaging. Notably, the experimentally measured T_{1w} is complex, susceptible to the underlying CEST, NOE and MT effects as well as intracellular viscosity, fraction of bound and free water molecule. For dilute amide protons and under the condition of weak RF saturation, the observed T_{1w} provides a reasonable estimation of the effective relaxation rate under which the dilute CEST effect relaxes. This is confirmed by the finding that the multiple regression analysis based on the experimentally measured T_{1w} highly correlates with the intrinsic APTR inhomogeneity. In addition, there may be means to shorten the scan time. Our study used an inversion recovery sequence and measured quantitative T_1 map, which may be replaced by the look-locker MRI approach (Freeman et al., 1998). An alternative means is to test whether a T_{1w}-weighted image can provide satisfactory correction to further reduce the total scan time. However, depending on the stroke onset time, there may be presence of edema, which may cause water content change and heterogeneous amide proton distribution in the brain. In addition, APT MRI is susceptible to MT and NOE effects, which confound its quantification. Under such conditions, the emerging field of quantitative CEST (qCEST) MRI may eventually allow us to measure tissue acidosis independent of water content and relaxation changes. However, absolute pH imaging has to fully account for all these confounding factors within a minimal scan time, which could be challenging. The proposed MRAPT analysis is expeditious to acquire, simple to implement, yet provides refined lesion stratification. Future studies will investigate whether ΔMRAPTR can map the amount of pH change (ΔpH) from the baseline.

There are a few limitations of our current study. Our study here chose a relatively reproducible filament stroke model to refine pH imaging and aid ischemic tissue classification. Because the commonly used staining techniques (e.g. H&E and TTC) are not suitable for characterizing tissue acidification and injury in the first few hours, no pH histology was obtained in our current study. Nevertheless, our findings of severity of pH drop from penumbral tissue and ischemic core are in good agreement with that of Back et al. (Back et al., 2000). Our study also showed ischemic penumbra and benign oligemia have significant pH difference, not cerebral blood flow, consistent with the clinical observation of Harston et al. (Harston et al., 2015) It is worthwhile to mention that our animal system has excellent field homogeneity. Indeed, after relaxation and MT corrections, MRAPT images appear homogeneous across the intact brain tissue, and we did not perform additional field inhomogeneity correction. Field correction may be necessary when translating pH MRI to study large animal models and stroke patients (Kim et al., 2009; Scheidegger et al., 2011; Sun et al., 2007a; Zhou et al., 2008). In addition, our study chose a filament stroke model, which induces severe hypoperfusion with poor collateral circulation, causing large infarction days later. Nevertheless, our acute stroke imaging results are consistent with those reported by Harston et al., who showed that when confined to the grey matter perfusion deficit, intracellular pH, but not cerebral blood flow, differs between tissue that infarcted and tissue that survived (Harston et al., 2015). Although embolic stroke model may better mimic pathophysiological events in acute stroke patients, it is more variable than filament stroke model. Because our study aims to first develop the MRAPT MRI technique to enhance the pH specificity of APT MRI for refined lesion delineation, we chose a relatively reproducible stroke model and imaged at a single time point. Built on our results that demonstrate the superiority of the proposed MRAPT MRI over the routine MTR_{asym} image in the stratification of heterogeneous metabolic disruption in the ischemic tissue, our future studies will investigate how the enhanced pH MRI helps to elucidate regional ischemic tissue response to recanalization and neuroprotective treatments and ultimately, translate it to the acute stroke setting (Leslie-Mazwi et al., 2016; Li et al., 2010).

6. Conclusion

Our study here shows that the proposed MRAPT MRI effectively minimized the non-acidosis related heterogeneity commonly observed in the routine pH-weighted MTR_{asym} map, resulting in substantially enhanced pH specificity. We found that diffusion lesion suffered more aggravated acidosis than the perfusion/diffusion lesion mismatch. Importantly, the MRAPT analysis allows semi-automatic lesion segmentation, which refines the conventional perfusion/diffusion lesion mismatch into hypoperfused and metabolically challenged penumbra (i.e., pH/diffusion mismatch) and benign oligemia with little acidification.

Acknowledgments

This study was supported by research grants from National Natural Science Foundation of China 81471721 (to Guo), National Science Foundation for Distinguished Young Scholars (to Ji), National Institutes of Health R21NS085574 and R01NS083654 (to Sun).

REFERENCES

Alsop DC, Detre JA. Multisection cerebral blood flow MR imaging with continuous arterial spin labeling. Radiology. 1998; 208:410–416. [PubMed: 9680569]

An H, Ford AL, Chen Y, Zhu H, Ponisio R, Kumar G, Shanechi AM, Khoury N, Vo KD, Williams J, Derdeyn CP, Diringer MN, Panagos P, Powers WJ, Lee J-M, Lin W. Defining the Ischemic Penumbra Using Magnetic Resonance Oxygen Metabolic Index. Stroke. 2015; 46:982–988. [PubMed: 25721017]

Back T, Hoehn M, Mies G, Busch E, Schmitz B, Kohno K, Hossmann K. Penumbral tissue alkalosis in focal cerebral ischemia: relationship to energy metabolism, blood flow, and steady potential. Ann Neurol. 2000; 47:485–492. [PubMed: 10762160]

Cai K, Haris M, Singh A, Kogan F, Greenberg JH, Hariharan H, Detre JA, Reddy R. Magnetic resonance imaging of glutamate. Nat Med. 2012; 18:302–306. [PubMed: 22270722]

Chang L, Shirane R, Weinstein PR, James TL. Cerebral Metabolite Dynamics during Temporary Complete Ischemia in Rats Monitored by Time-Shared 1H and 31P NMR Spectroscopy. Magn Reson Med. 1990; 13:6–13. [PubMed: 2319935]

Cheung JS, Wang EF, Wang XY, Sun PZ. Effect of ISODATA dimensionality on spatiotemporal evolution of ischemic brain injury in acute ischemic stroke Intl. Soc. Mag. Reson. Med., Montréal, Québec, Canada. 2011:2599.

Cheung JS, Wang EF, Zhang XA, Manderville E, Lo EH, Sorensen AG, Sun PZ. Fast radio-frequency enforced steady state (FRESS) spin echo MRI for quantitative T2 mapping: minimizing the apparent repetition time (TR) dependence for fast T2 measurement. NMR Biomed. 2012; 25:189–194. [PubMed: 21755552]

de Graaf RA, Brown PB, McIntyre S, Nixon TW, Behar KL, Rothman DL. High magnetic field water and metabolite proton T1 and T2 relaxation in rat brain in vivo. Magn Reson Med. 2006; 56:386–394. [PubMed: 16767752]

Desmond KL, Stanisz GJ. Understanding quantitative pulsed CEST in the presence of MT. Magn Reson Med. 2012; 67:979–990. [PubMed: 21858864]

Freeman AJ, Gowland PA, Mansfield P. Optimization of the ultrafast look-locker echo-planar imaging T1 mapping sequence. Magn Reson Imag. 1998; 16:765–772.

Harston GWJ, Tee YK, Blockley N, Okell TW, Thandeswaran S, Shaya G, Sheerin F, Cellerini M, Payne S, Jezzard P, Chappell M, Kennedy J. Identifying the ischaemic penumbra using pH-weighted magnetic resonance imaging. Brain. 2015; 138:36–42. [PubMed: 25564491]

Heo H-Y, Zhang Y, Jiang S, Lee D-H, Zhou J. Quantitative assessment of amide proton transfer (APT) and nuclear overhauser enhancement (NOE) imaging with extrapolated semisolid magnetization transfer reference (EMR) signals: II. Comparison of three EMR models and application to human brain glioma at 3 Tesla. Magn Reson Med. 2016; 75:1630–1639. [PubMed: 26033553]

Jin T, Wang P, Zong X, Kim S-G. MR imaging of the amide-proton transfer effect and the pH-insensitive nuclear overhauser effect at 9.4 T. Magn Reson Med. 2013; 69:760–770. [PubMed: 22577042]

Jokivarsi KT, Gröhn HI, Gröhn OH, Kauppinen RA. Proton transfer ratio, lactate, and intracellular pH in acute cerebral ischemia. Magn Reson Med. 2007; 57:647–653. [PubMed: 17390356]

Jokivarsi KT, Hiltunen Y, Grohn H, Tuunanen P, Grohn OHJ, Kauppinen RA. Estimation of the Onset Time of Cerebral Ischemia Using T1{rho} and T2 MRI in Rats. Stroke. 2010; 41:2335–2340. [PubMed: 20814006]

Jones CK, Huang A, Xu J, Edden RAE, Schar M, Hua J, Oskolkov N, Zaca D, Zhou J, McMahon MT, Pillai JJ, van Zijl PCM. Nuclear Overhauser enhancement (NOE) imaging in the human brain at 7 T. NeuroImage. 2013; 77:114–124. [PubMed: 23567889]

Kidwell CS, Alger JR, Saver JL. Evolving paradigms in neuroimaging of the ischemic penumbra. Stroke. 2004; 35:2662–2665. [PubMed: 15472112]

Kim M, Gillen J, Landman BA, Zhou J, van Zijl PCM. Water saturation shift referencing (WASSR) for chemical exchange saturation transfer (CEST) experiments. Magn Reson Med. 2009; 61:1441–1450. [PubMed: 19358232]

Leslie-Mazwi TM, Hirsch JA, Falcone GJ, et al. ENdovascular stroke treatment outcomes after patient selection based on magnetic resonance imaging and clinical criteria. JAMA Neurology. 2016; 73:43–49. [PubMed: 26524074]

Li M, Inoue K, Branigan D, Kratzer E, Hansen JC, Chen JW, Simon RP, Xiong Z-G. Acid-Sensing Ion Channels in Acidosis-Induced Injury of Human Brain Neurons. J Cereb Blood Flow Metab. 2010; 30:1247–1260. [PubMed: 20216553]

Makela HI, Kettunen MI, Grohn OH, Kauppinen RA. Quantitative $T1_\rho$ and magnetic transfer magnetic resonance imaging of acute cerebral ischemia in the rat. J. Cereb. Blood Flow Metab. 2002; 22:547–558. [PubMed: 11973427]

McVicar N, Li AX, Goncalves DF, Bellyou M, Meakin SO, Prado MAM, Bartha R. Quantitative tissue pH measurement during cerebral ischemia using amine and amide concentration-independent detection (AACID) with MRI. J Cereb Blood Flow Metab. 2014; 34:690–698. [PubMed: 24496171]

Moon RB, Richards JH. Determination of intracellular pH by ^{31}P magnetic resonance. J. Biol. Chem. 1973; 248:7276–7278. [PubMed: 4743524]

Mori S, van Zijl PCM. Diffusion weighting by the trace of the diffusion tensor within a single scan. Magn Reson Med. 1995; 33:41–52. [PubMed: 7891534]

Ojugo A, McSheehy P, McIntyre D, McCoy C, Stubbs M, Leach MO, Judson IR, Griffiths JR. Measurement of the extracellular pH of solid tumours in mice by magnetic resonance spectroscopy: a comparison of exogenous 19F and 31P probes. NMR Biomed. 1999; 12:495–504. [PubMed: 10668042]

Scheidegger R, Vinogradov E, Alsop DC. Amide proton transfer imaging with improved robustness to magnetic field inhomogeneity and magnetization transfer asymmetry using saturation with frequency alternating RF irradiation. Magn Reson Med. 2011; 66:1275–1285. [PubMed: 21608029]

Scheidegger R, Wong ET, Alsop DC. Contributors to contrast between glioma and brain tissue in chemical exchange saturation transfer sensitive imaging at 3 Tesla. NeuroImage. 2014; 99:256–268. [PubMed: 24857712]

Shen Q, Huang S, Duong TQ. T2*-weighted fMRI time-to-peak of oxygen challenge in ischemic stroke. J Cereb Blood Flow Metab. 2016; 36:283–291. [PubMed: 26661164]

Sheth VR, Li Y, Chen LQ, Howison CM, Flask CA, Pagel MD. Measuring in vivo tumor pHe with CEST-FISP MRI. Magn Reson Med. 2012; 67:760–768. [PubMed: 22028287]

Shu CY, Sanganahalli BG, Coman D, Herman P, Rothman DL, Hyder F. Quantitative β mapping for calibrated fMRI. NeuroImage. 2016; 126:219–228. [PubMed: 26619788]

Siesjo BK. Pathophysiology and treatment of focal cerebral ischemia: Part I: Pathophysiology. J. Neurosurg. 1992; 77:169–184. [PubMed: 1625004]

Sun PZ, Cheung JS, Wang E, Benner T, Sorensen AG. Fast multi-slice pH-weighted chemical exchange saturation transfer (CEST) MRI with unevenly segmented RF irradiation. Magn Reson Med. 2011a; 65:588–594. [PubMed: 20872859]

Sun PZ, Cheung JS, Wang EF, Lo EH. Association between pH-weighted endogenous amide proton chemical exchange saturation transfer MRI and tissue lactic acidosis during acute ischemic stroke. J. Cereb. Blood Flow Metab. 2011b; 31:1743–1750. [PubMed: 21386856]

Sun PZ, Farrar CT, Sorensen AG. Correction for artifacts induced by B0 and B1 field inhomogeneities in pH-sensitive chemical exchange saturation transfer (CEST) imaging. Magn Reson Med. 2007a; 58:1207–1215. [PubMed: 17969015]

Sun PZ, Lu J, Wu Y, Xiao G, Wu R. Evaluation of the dependence of CEST-EPI measurement on repetition time, RF irradiation duty cycle and imaging flip angle for enhanced pH sensitivity. Phys Med Biol. 2013; 58:N229–N240. [PubMed: 23939228]

Sun PZ, Sorensen AG. Imaging pH using the chemical exchange saturation transfer (CEST) MRI: correction of concomitant RF irradiation effects to quantify CEST MRI for chemical exchange rate and pH. Magn Reson Med. 2008; 60:390–397. [PubMed: 18666128]

Sun PZ, van Zijl PCM, Zhou J. Optimization of the irradiation power in chemical exchange dependent saturation transfer experiments. J Magn Reson. 2005; 175:193–200. [PubMed: 15893487]

Sun PZ, Wang E, Cheung JS. Imaging acute ischemic tissue acidosis with pH-sensitive endogenous amide proton transfer (APT) MRI – Correction of tissue relaxation and concomitant RF irradiation effects toward mapping quantitative cerebral tissue pH. NeuroImage. 2012; 60:1–6. [PubMed: 22178815]

Sun PZ, Zhou J, Huang J, van Zijl P. Simplified quantitative description of amide proton transfer (APT) imaging during acute ischemia. Magn Reson Med. 2007b; 57:405–410. [PubMed: 17260362]

Sun PZ, Zhou J, Sun W, Huang J, van Zijl PC. Detection of the ischemic penumbra using pH-weighted MRI. J Cereb Blood Flow Metab. 2007c; 27:1129–1136. [PubMed: 17133226]

Utting JF, Thomas DL, Gadian DG, Helliar RW, Lythgoe MF, Ordidge RJ. Understanding and optimizing the amplitude modulated control for multiple-slice continuous arterial spin labeling. Magn Reson Med. 2005; 54:594–604. [PubMed: 16086330]

Ward KM, Aletras AH, Balaban RS. A new class of contrast agents for MRI based on proton chemical exchange dependent saturation transfer (CEST). J Magn Reson. 2000; 143:79–87. [PubMed: 10698648]

Woessner DE, Zhang S, Merritt ME, Sherry AD. Numerical solution of the Bloch equations provides insights into the optimum design of PARACEST agents for MRI. Magn Reson Med. 2005; 53:790–799. [PubMed: 15799055]

Wu R, Liu C, Liu P, Sun PZ. Improved measurement of labile proton concentration-weighted chemical exchange rate (kws) with experimental factor-compensated and T1-normalized quantitative chemical exchange saturation transfer (CEST) MRI. Contrast Media Mol Imaging. 2012; 7:384–389. [PubMed: 22649044]

Zhang X-Y, Wang F, Afzal A, Xu J, Gore JC, Gochberg DF, Zu Z. A new NOE-mediated MT signal at around − 1.6 ppm for detecting ischemic stroke in rat brain. Magn Reson Imaging. 2016; 34:1100–1106. [PubMed: 27211260]

Zhao X, Wen Z, Huang F, Lu S, Wang X, Hu S, Zu D, Zhou J. Saturation power dependence of amide proton transfer image contrasts in human brain tumors and strokes at 3 T. Magn Reson Med. 2011; 66:1033–1041. [PubMed: 21394783]

Zhou J, Blakeley JO, Hua J, Kim M, Laterra J, Pomper MG, van Zijl PCM. Practical data acquisition method for human brain tumor amide proton transfer (APT) imaging. Magn Reson Med. 2008; 60:842–849. [PubMed: 18816868]

Zhou J, Payen JF, Wilson DA, Traystman RJ, van Zijl PC. Using the amide proton signals of intracellular proteins and peptides to detect pH effects in MRI. Nat Med. 2003; 9:1085–1090. [PubMed: 12872167]

Zhou J, Wilson DA, Sun PZ, Klaus JA, van Zijl PCM. Quantitative description of proton exchange processes between water and endogenous and exogenous agents for WEX, CEST, and APT experiments. Magn Reson Med. 2004; 51:945–952. [PubMed: 15122676]

Zhu X-H, Chen JM, Tu T-W, Chen W, Song S-K. Simultaneous and noninvasive imaging of cerebral oxygen metabolic rate, blood flow and oxygen extraction fraction in stroke mice. NeuroImage. 2013; 64:437–447. [PubMed: 23000789]

Zong X, Wang P, Kim S-G, Jin T. Sensitivity and Source of Amine-Proton Exchange and Amide-Proton Transfer Magnetic Resonance Imaging in Cerebral Ischemia. Magn Reson Med. 2014; 71:118–132. [PubMed: 23401310]

- Magnetization transfer and relaxation-normalized APT (MRAPT) MRI is pH specific.
- pH MRI shows graded metabolic disruption in acute ischemic tissue.
- pH MRI delineates metabolic penumbra from benign oligemia.
- pH MRI augments perfusion and diffusion imaging for refined tissue classification.

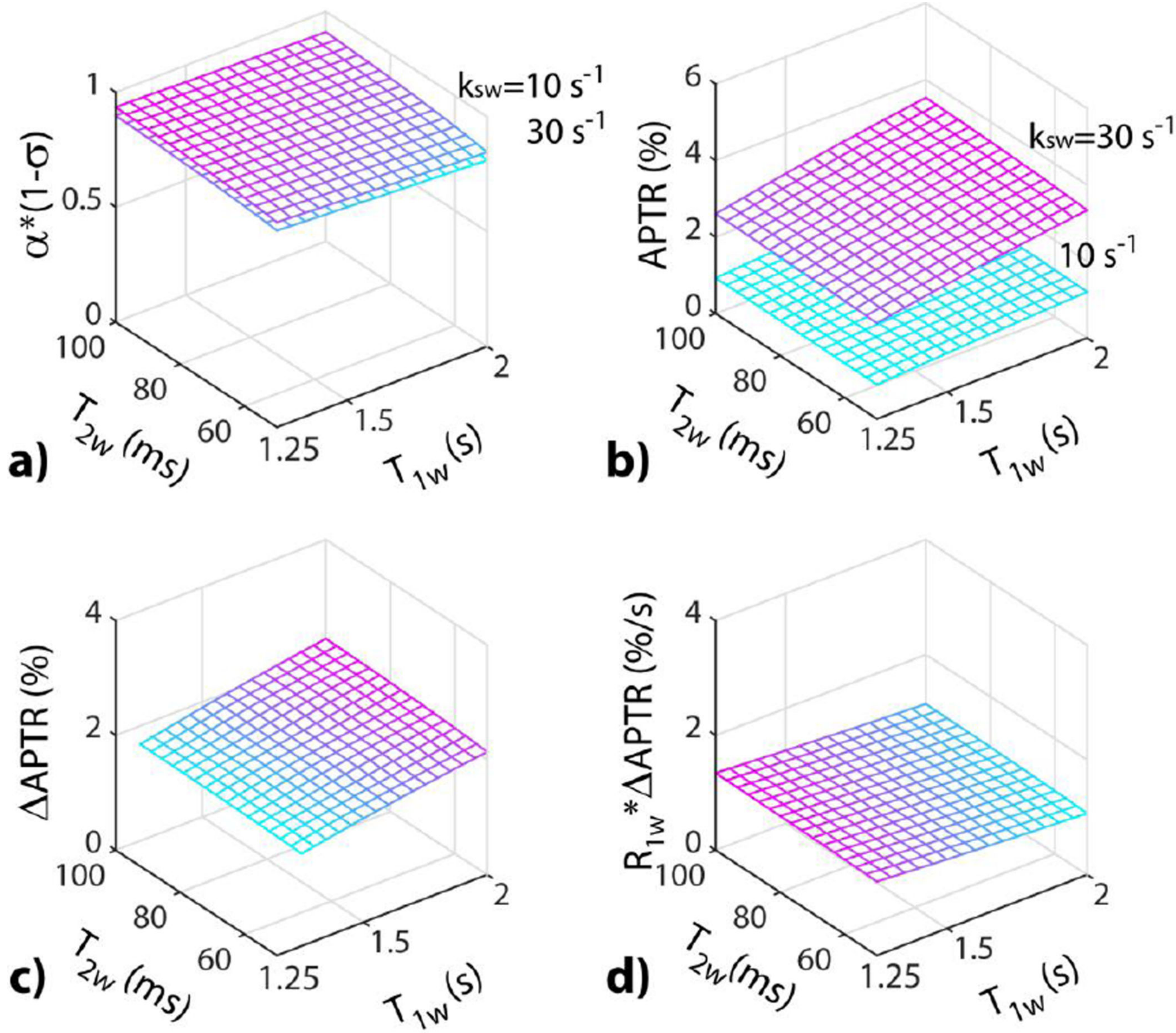

Fig. 1.

Simulation of T_{1w}-normalized APT MRI for two representative exchange rates of 30 and 10 s^{-1} at 4.7 Tesla (B_1=0.75 μT). a) APT MRI experimental factor as a function of T_{1w} and T_{2w}. b) pH-sensitive APT ratio (APTR) as a function of T_{1w} and T_{2w}. c) APTR pH contrast (ΔAPTR) as a function of T_{1w} and T_{2w}. d) T_{1w}normalized ΔAPTR as a function of T_{1w} and T_{2w}, showing reduced sensitivity to relaxation rates.

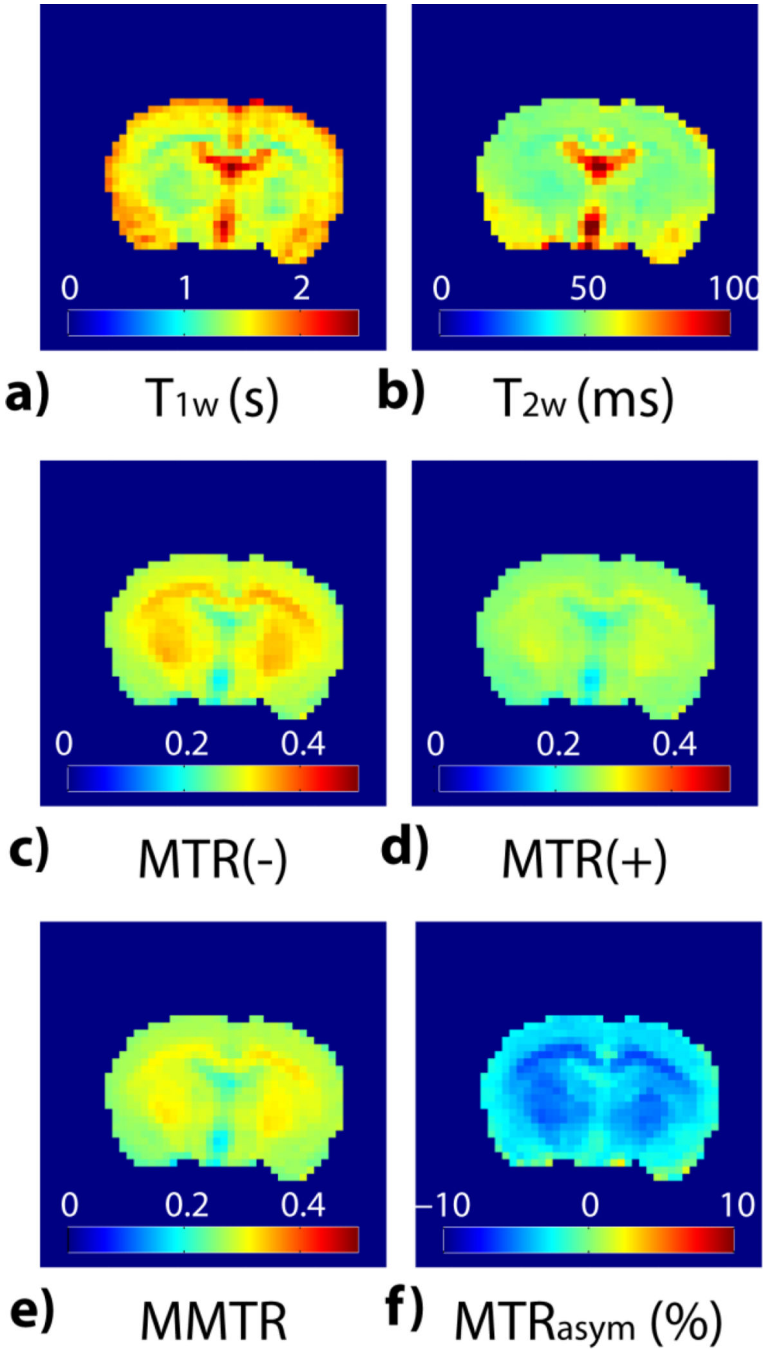

Fig. 2.

Multi-parametric MRI images from a representative normal rat. a) Longitudinal relaxation time T_{1w} map. b) Transverse relaxation time T_{2w} map. c) MTR(−) image (i.e., MTR at −3.5 ppm). d) MTR(+) image (i.e., MTR at +3.5 ppm). e) MMTR image (i.e., mean of MTR(±) images). f) pH-weighted MTR_{asym} image.

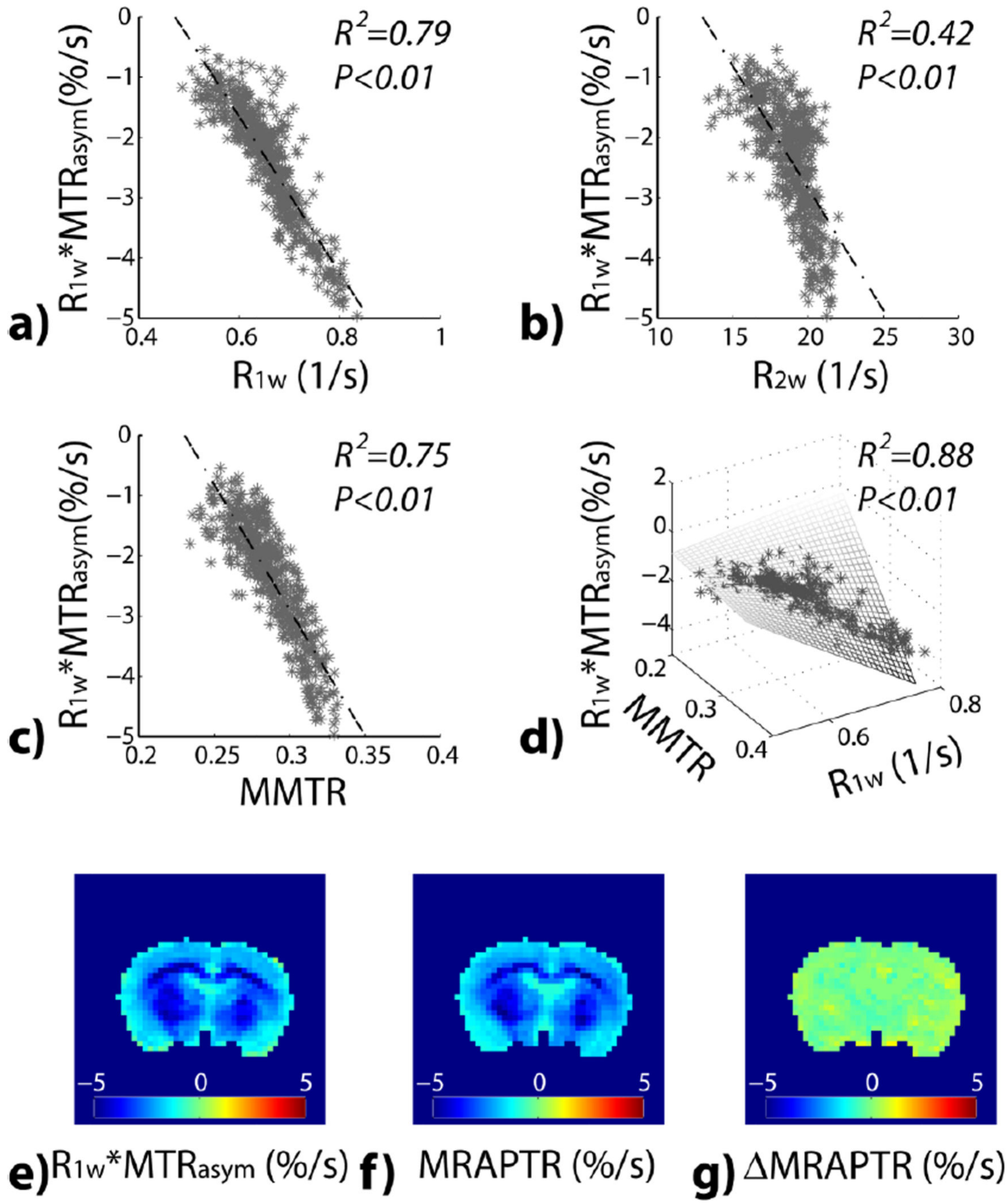

Fig. 3.

Pixel-wise regression analysis between R_{1w}-scaled MTR_{asym} with multiple MRI parameters from a representative normal rat. a) $R_{1w}*MTR_{asym}$ as a function of R_{1w}. b) $R_{1w}*MTR_{asym}$ as a function of R_{2w}. c) $R_{1w}*MTR_{asym}$ as a function of MMTR. d) $R_{1w}*MTR_{asym}$ as a function of R_{1w} and MMTR. e) $R_{1w}*MTR_{asym}$ image. f) R_{1w} and MMTR-based multiple regression prediction of $R_{1w}*MTR_{asym}$ image. g) ΔMRAPTR image, the difference between the experimentally measured $R_{1w}*MTR_{asym}$ image and the multiple regression prediction.

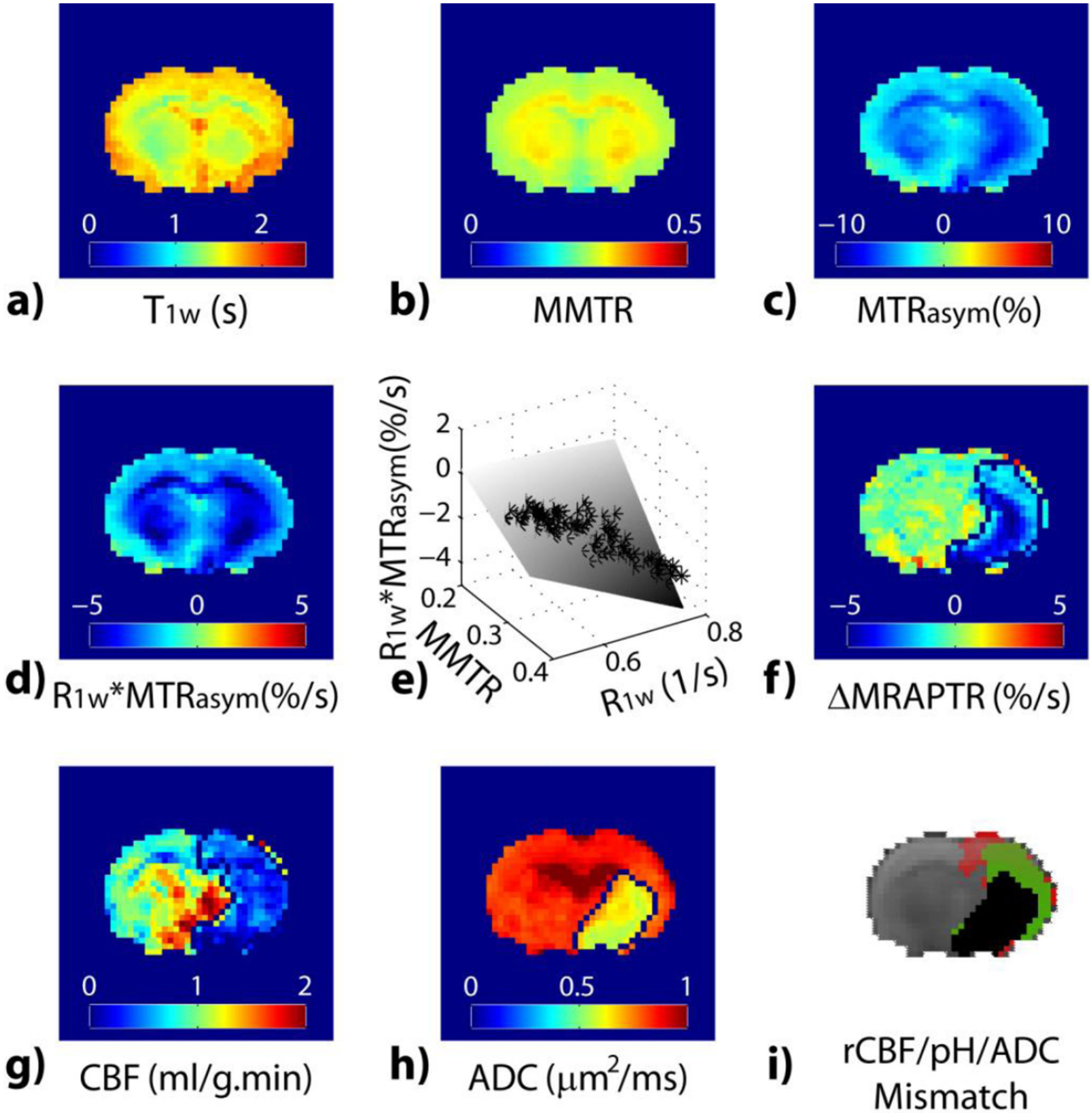

Fig. 4.

MRAPT MRI analysis from a representative acute stroke rat. a) Parametric T_{1w} map. b) MMTR image c) pH-weighted MTR_{asym} image. d) pH-weighted $R_{1w}*MTR_{asym}$ image. e) Multiple regression analysis of $R_{1w}*MTR_{asym}$ as a function of R_{1w} and MMTR. f) pH-sensitive ΔMRAPTR image. g) CBF map. h) ADC map. i) Color-coded perfusion (red), pH (green) and diffusion (black) lesions.

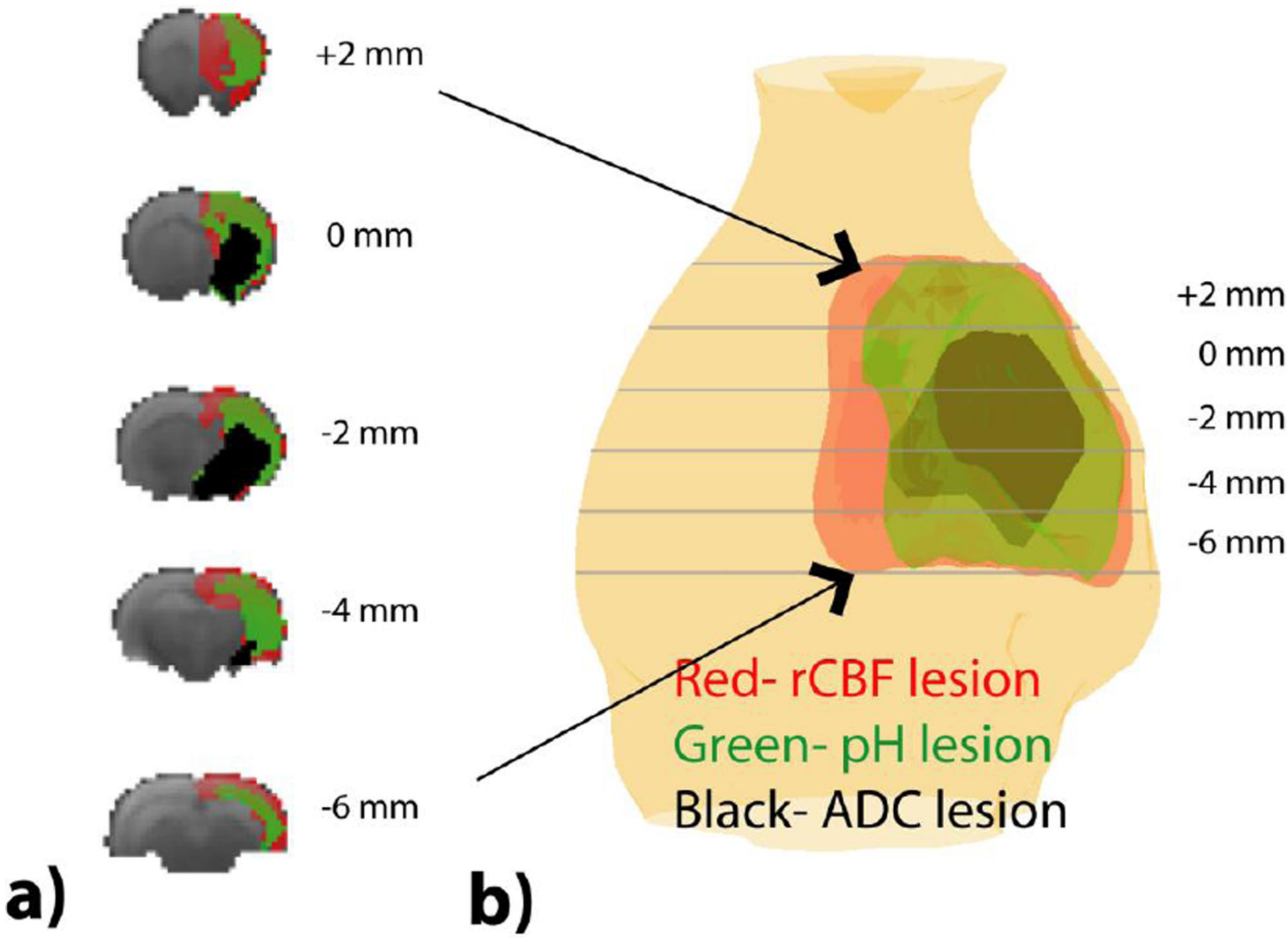

Fig. 5.

Multi-parametric MRI segmentation of ischemic tissue injury. a) Multi-slice perfusion, pH and diffusion lesion segmentation. b) 3D volume rendering of ischemic lesions overlaid on a structural scan.

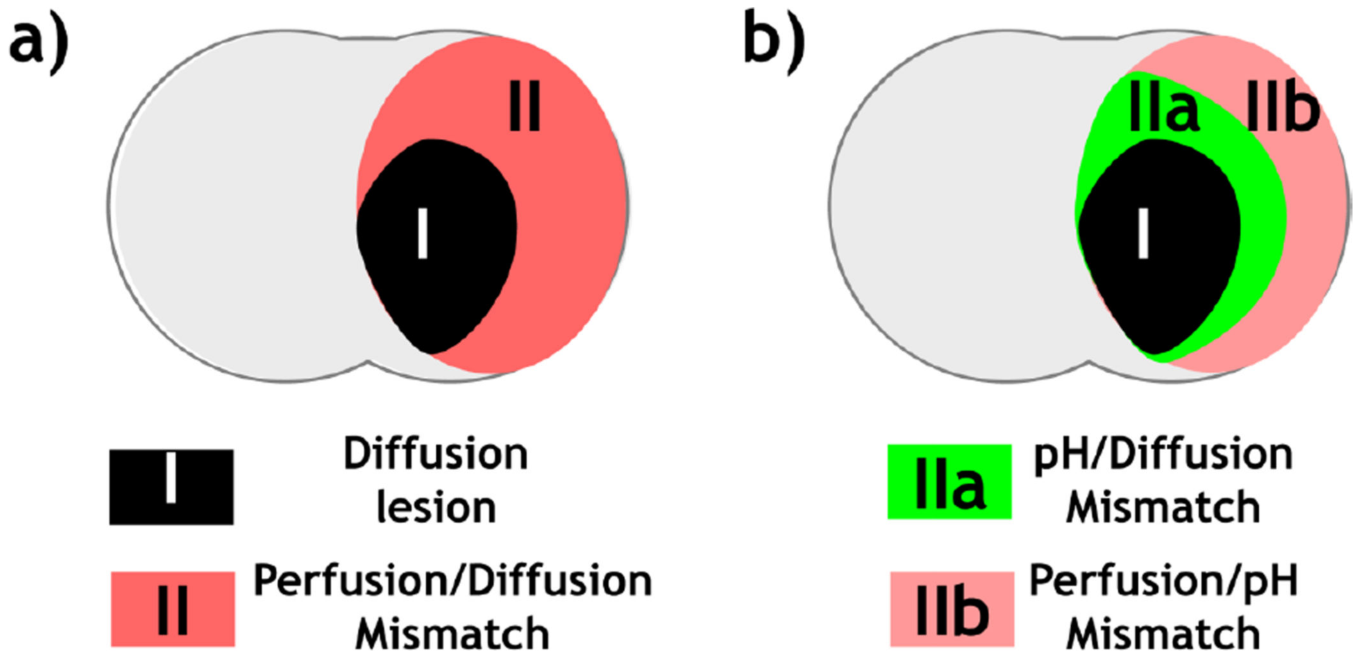

Fig. 6.

pH-aided ischemic lesion classification. a) Routine perfusion/diffusion MRI-based tissue stratification. b) pH MRI refines perfusion/diffusion lesion mismatch into two areas: 1) hypoperfused and acidic penumbra (Area IIa) and 2) benign oligemia area with little acidosis (Area IIb).

Table 1

The rCBF, pH and ADC show significant difference between ADC lesion and PWI/ADC mismatch.

	DWI lesion (Area I)	**PWI/DWI mismatch (Area II)**	**PWI/DWI mismatch vs. DWI lesion** ***Mean Difference (P value)***
rCBF	0.51 ± 0.11	0.58 ± 0.12	0.07 (0.001*)
ADC(μm^2/ms)	0.64 ± 0.04	0.85 ± 0.04	0.21 (<0.001*)
ΔMRAPTR (%/s)	−1.05 ± 0.29	−0.32 ± 0.18	0.72 (<0.001*)

Table 2

Comparison of multiple indices in refined lesion segmentation. a) One-way ANOVA shows significant change in rCBF, pH and ADC among ADC lesion, pH/ADC and PWI/pH mismatch. b) One-way ANOVA shows pH resolves all three regions: ADC lesion, pH/ADC mismatch and PWI/pH mismatch while rCBF and ADC have limited ability to refine the lesion zones.

a

	DWI lesion (Area I)	**pH/DWI mismatch (Area IIa)**	**PWI/pH mismatch (Area IIb)**	**One-way ANOVA** ***F (P value)***
rCBF	0.51 ± 0.11	0.56 ± 0.14	0.62 ± 0.11	4.24 (0.019*)
ADC(μm^2/ms)	0.64 ± 0.04	0.83 ± 0.05	0.84 ± 0.05	128.07 (<0.001*)
ΔMRAPTR (%/s)	−1.05 ± 0.29	−0.67 ± 0.27	−0.04 ± 0.14	89.17 (<0.001*)

b

	DWI lesion vs. pH/DWI mismatch (Areas I vs. IIa) ***Mean Difference (P value)***	**DWI lesion vs. PWI/pH mismatch (Areas I vs. IIb)** ***Mean Difference (P value)***	**PWI/pH vs. pH/DWI mismatch (Areas IIa vs. IIb)** ***Mean Difference (P value)***
rCBF	0.05 (0.370)	0.11 (0.01*)	0.06 (0.274)
ADC(μm^2/ms)	0.18 (<0.001*)	0.20 (<0.001*)	0.02 (0.490)
ΔMRAPTR (%/s)	0.37 (<0.001*)	1.01(<0.001*)	0.63 (<0.001*)